Journal of Alloys and Compounds 509 (2011) 2478–2486

Contents lists available at ScienceDirect

Journal of Alloys and Compounds

journal homepage: www.elsevier.com/locate/jallcom

Experimental investigation and thermodynamic modeling of the phase equilibria at the Mg–Ni side in the La–Mg–Ni ternary system

Qian Li*, Xu Zhang, Xue-Hui An, Shuang-Lin Chen, Jie-Yu Zhang

Shanghai Key Laboratory of Modern Metallurgy & Materials Processing, Shanghai University, Shanghai 200072, China

ARTICLE INFO

Article history:
Received 23 April 2010
Received in revised form 19 July 2010
Accepted 10 November 2010
Available online 18 November 2010

Keywords:
Hydrogen absorbing materials
Thermodynamic properties
Phase diagrams
Calphad

ABSTRACT

The La–Mg–Ni system is considered as one of the most promising candidates for the hydrogen storage alloys, and most of hydrogen storage phases in the La–Mg–Ni ternary system are mainly located near the Mg–Ni side. The present work focused on clarifying the phase relationships at the Mg–Ni side using the Calphad method. The thermodynamic descriptions of phase relationship were established on the available literature data together with our experimental results. Several key specimens were selected, synthesized and annealed at 773 K, 973 K and 1173 K to confirm the accuracy of the phase diagram calculated from the ternary thermodynamic description. Inductively coupled plasma, X-ray diffraction and scanning electron microscopy with electron dispersive spectrometry were used to analyze the alloys. The acceptable agreement on the equilibrium phases between the experimental and calculated results suggested the reliability of the assessed thermodynamic descriptions of phase relationship. The optimized phase equilibrium and thermodynamic information were successfully used to discuss the synthesized technological parameter of the La–Mg–Ni hydrogen storage alloys.

1. Introduction

Ternary La–Mg–Ni alloys are known for their good ability to absorb/desorb hydrogen in the solid state and electrochemical property as electrode materials [1–4]. They are considered as the potential promising candidates for their high hydrogen storage capacity, light weight and low cost. Many binary and ternary hydrogen storage phases in La–Mg–Ni system locate at the Mg–Ni side [1–9], such as Mg_2Ni, $La_2(Mg_{1-x}Ni_x)_{17}$, $(La_{1-x}Mg_x)Ni_3$, $(La_{1-x}Mg_x)Ni_2$, $(La_{1-x}Mg_x)_2Ni_7$ and $LaMg_2Ni$. The AB_3-type and A_2B_7-type hydrogen storage alloys were extensively studied due to the phases $(La_{1-x}Mg_x)Ni_3$ and $(La_{1-x}Mg_x)_2Ni_7$ in Ni-rich corner with a good electrochemical property [1–5]. La_2Mg_{17} and Mg_2Ni in Mg-rich corner are also investigated because of their good hydrogen storage performance [6,7]. However, a more systematical and particular description on phase diagram of the La–Mg–Ni ternary system is needed to explore its thermodynamics. The phase equilibrium and thermodynamic information will be useful for designing the optimal hydrogen storage alloy composition and heat-treatment condition in order to control phase formation during the synthetic process and to further improve the properties of alloys. For example, Denys et al. [10] experimentally determined the ternary phase diagram of Mg–Ni–Mn system and applied the phase diagram to investigate the properties of the hydrogen storage phases in the ternary systems. However, the conventional experimental determination of a ternary phase diagram is very time consuming. A more advanced and effective method for the design of multi-component hydrogen storage alloys is to couple the thermodynamic calculation of phase diagram (CALPHAD) with experimental determination [11,12].

In this study, utilizing the available data reported in literatures coupled with our experimental results, the Mg–Ni side in the La–Mg–Ni system was thermodynamically assessed by the CALPHAD approach. Then this obtained consistent thermodynamic description was used to discuss the synthesized technological parameter of the La–Mg–Ni hydrogen storage alloys, which were verified by the experimental results published in literatures.

2. Thermodynamic description in the literature

2.1. Binary systems

The La–Mg phase diagram was assessed by Nayeb-Hashemi and Clark [13], and five intermetallic compounds including $LaMg_{12}$, La_2Mg_{17}, $LaMg_3$, $LaMg_2$ and LaMg were reported. Giovannini et al. [14] investigated the Mg-rich region and found a stoichiometric phase, La_5Mg_{41}, of which the structure is very similar to that of the La_2Mg_{17} phase. However, many researchers believed that only

* Corresponding author at: School of Materials Science and Engineering, Shanghai University, 149 Yanchang Road, Shanghai 200072, China. Tel.: +86 21 56334045; fax: +86 21 56338065.
E-mail addresses: shuliqian@shu.edu.cn, qian246@hotmail.com (Q. Li).

0925-8388/$ – see front matter © 2010 Elsevier B.V. All rights reserved.
doi:10.1016/j.jallcom.2010.11.057

Table 1
The unary, binary and ternary phases at the Mg–Ni side of La–Mg–Ni system from literatures.

Phase	Pearson symbol/prototype	Stability range (K)	Space group	Lattice parameters (nm)		
				a	*b*	*c*
Mg	hP2-Mg	<923 K	$P6_3/mmc$	0.3209		0.5211
Ni	cF4-Cu	<1728 K	$Fm\bar{3}m$	0.3523		
LaMg	cP2-CsCl	<1018 K	$Pm\bar{3}m$	0.3965		
$LaMg_2$	cF24-$MgCu_2$	998–1048 K	$Fd\bar{3}m$	0.8774		
$LaMg_3$	cF16-BiF_3	<1071 K	$Fm\bar{3}m$	0.7494		
$La_2(Mg_{1-x}Ni_x)_{17}$	hP38-Th_2Ni_{17}	<?	$P6_3/mmc$			
La_2Mg_{17}, $x=0$		<943 K		1.0350		1.0280
$LaMg_{12}$	oI338-$CeMg_{12}$	<913 K	Im*mm*	1.033	1.033	7.749
Mg_2Ni	hP18-Mg_2Ni	<1033 K	$P6_222$	0.5205		1.3236
$MgNi_2$	hP24-$MgNi_2$	<1420 K	$P6_3/mmc$	0.4824		1.5826
$LaNi_5$	hP6-$CaCu_5$	<1623 K	$P6/mmm$	0.5016		0.3983
La_7Ni_{16}	tI46-La_7Ni_{16}	<987 K	$I\bar{4}2m$	0.7355		1.451
La_2Ni_3	oC20-La_2Ni_3	<961 K	*Cmca*	0.5113	0.9731	0.7907
$(La_{1-x}Mg_x)_2Ni_7$		<?				
βLa_2Ni_7, $x=0$	hR18-Gd_2Co_7	1263–1287 K	$R\bar{3}m$	0.5056		3.698
αLa_2Ni_7, $x=0$	hP36-Ce_2Ni_7	<1263 K	$P6_3/mmc$	0.5058		2.471
$(La_{1-x}Mg_x)Ni_3$	hR36-$PuNi_3$	<?	$R\bar{3}m$			
$LaNi_3$, $x=0$		<1084 K		0.5086		2.501
$LaMg_2Ni_9$, $x=0.67$		<?		0.4923		2.3866
$(La_{1-x}Mg_x)Ni_2$	cF24-Cu_2Mg	<?	$Fd\bar{3}m$			
$LaNi_2$, $x=0$	cF24-Cu_2Mg	Metastable	$Fd\bar{3}m$	0.7247		
$LaMgNi_4$, $x=0.5$	cF24-$MgCu_4Sn$	<?	$F\bar{4}3m$	0.717		
$LaMg_2Ni$	oC16-$CuMgAl_2$	<903 K	*Cmcm*	0.4277	1.0303	0.8360

the La_2Mg_{17} would probably be stable at low temperature [15]. Guo et al. [16] got the thermodynamic parameters with a good self-consistency by reassessing the La–Mg system using CALPHAD approach.

The Mg–Ni phase diagram containing $MgNi_2$ and Mg_2Ni two intermetallic compounds was assessed by Nayeb-Hashemi and Clark [17], and then reassessed and got the thermodynamic parameters with good self-consistency in work reported by Jacobs and Spencer [18]. Later, Islam and Medraj [19] assessed the system again because they considered that thermodynamic parameters from Jacob and Spencer were complex and not suitable for the Mg–Ni–Ca ternary system. However, the Mg–Ni system assessed by Islam and Medraj [19] was not consistent with the thermodynamic properties, especially the measured heat capacities of C16 Mg_2Ni and Laves-C36 $MgNi_2$ phases.

The La–Ni binary system contains nine intermetallic compounds which are La_3Ni, La_7Ni_3, LaNi, La_2Ni_3, La_7Ni_{16}, $LaNi_3$, αLa_2Ni_7, βLa_2Ni_7 and $LaNi_5$. The phase diagram was reviewed early by Okamoto [20]. Based on previous work, Du et al. [21] and Dischinger and Schaller [22] assessed the La–Ni system and got a good agreement with experimental data. Dischinger and Schaller [22] reported a new binary stoichiometry La_4Ni_{17}, which was not found in any other literatures.

2.2. The La–Mg–Ni ternary system

Effenberg et al. [23] revised the phase relations involved in the Mg-rich corner of the isothermal section at 673 K and the liquidus surface according to the reported ternary compounds and the compiled literature data of the La–Mg–Ni ternary system. A ternary compound of $LaMg_2Ni$ was studied by Karonic et al. [24], who did not report the crystal structure. Di Chio et al. [8] measured the lattice constants of $LaMg_2Ni$ by XRD and reported its hydrogen absorption performance. Oesterreicher and Bittner [9], Guénée et al. [25] and Kadir et al. [26] investigated the compound $(La_{1-x}Mg_x)Ni_2$ and found that $(La_{1-x}Mg_x)Ni_2$ existed in the range of $0<x<0.67$. Kadir et al. [27] firstly used two different methods to synthesize a new ternary compound, $LaMg_2Ni_9$, with $PuNi_3$-type structure. Then, Liao et al. [2] studied the effect of La/Mg ratio on the crystal structures and electrochemical performances of $(La_xMg_{1-x})Ni_3(1/3<x<2/3)$ and found this series of alloys kept the $PuNi_3$-type structure with a large discharge capacity (~400 mAh/g). The $(La_{1-x}Mg_x)_2Ni_7$ alloy was investigated by Dong et al. [3] and Zhang [28], who found that La_2Ni_7 could dissolved about 5 at.% Mg at 1173 K and also had a large discharge capacity (~343.7 mAh/g).

Feufel et al. [29] and Schmid and Sommer [30] investigated the thermodynamic properties of liquid La–Mg–Ni alloys with associate model, respectively. De Negri et al. [31,32] investigated the phase relations of the La–Mg–Ni system with experimental measurements and plotted the isothermal section at 773 K. Zhang et al. [33] analyzed phase equilibria of the La–Mg–Ni bulk metallic glass system and obtained a complete thermodynamic description. Table 1 summarized the unary, binary and ternary phases at the Mg–Ni side of the La–Mg–Ni system from literatures.

3. Thermodynamic modeling

At the Mg–Ni side of the La–Mg–Ni system the thermodynamic models of the liquid, $La_2(Mg_{1-x}Ni_x)_{17}$, $LaMg_2Ni$, $(La_{1-x}Mg_x)Ni_2$, $(La_{1-x}Mg_x)Ni_3$ and $(La_{1-x}Mg_x)_2Ni_7$ phases need to be considered.

The Gibbs energy of the liquid is described by the substitutional solution model, as the following expression:

$$G^{\mathrm{Liq}} = x_{\mathrm{La}}{}^{\circ}G^{\mathrm{Liq}}_{\mathrm{La}} + x_{\mathrm{Mg}}{}^{\circ}G^{\mathrm{Liq}}_{\mathrm{Mg}} + x_{\mathrm{Ni}}{}^{\circ}G^{\mathrm{Liq}}_{\mathrm{Ni}} + RT(x_{\mathrm{La}}\ln x_{\mathrm{La}} + x_{\mathrm{Mg}}\ln x_{\mathrm{Mg}} + x_{\mathrm{Ni}}\ln x_{\mathrm{Ni}}) + {}^{E}G^{\mathrm{Liq}} \quad (1)$$

where x_{La}, x_{Mg} and x_{Ni} are the mole fractions of the pure elements La, Mg and Ni, respectively, ${}^{E}G^{\mathrm{Liq}}$ is the excess Gibbs energy and expressed by the Redlich–Kister polynomial,

$${}^{E}G^{\mathrm{Liq}} = x_{\mathrm{La}}x_{\mathrm{Mg}}\sum_k {}^{k}L^{\mathrm{Liq}}_{\mathrm{La,Mg}}(x_{\mathrm{La}}-x_{\mathrm{Mg}})^k + x_{\mathrm{La}}x_{\mathrm{Ni}}\sum_k {}^{k}L^{\mathrm{Liq}}_{\mathrm{La,Ni}}(x_{\mathrm{La}}-x_{\mathrm{Ni}})^k + x_{\mathrm{Mg}}x_{\mathrm{Ni}}\sum_k {}^{k}L^{\mathrm{Liq}}_{\mathrm{Mg,Ni}}(x_{\mathrm{Mg}}-x_{\mathrm{Ni}})^k + x_{\mathrm{La}}x_{\mathrm{Mg}}x_{\mathrm{Ni}}L^{\mathrm{Liq}}_{\mathrm{La,Mg,Ni}} \quad (2)$$

where ${}^{k}L^{\mathrm{Liq}}_{\mathrm{La,Mg}}$, ${}^{k}L^{\mathrm{Liq}}_{\mathrm{La,Ni}}$ and ${}^{k}L^{\mathrm{Liq}}_{\mathrm{Mg,Ni}}$ are the binary interaction parameters, $L^{\mathrm{Liq}}_{\mathrm{La,Mg,Ni}}$ is the ternary interaction parameter.

The ternary phase $LaMg_2Ni$ is a stoichiometric compound with $CuAl_2$Mg-type structure [8]. The Gibbs energy per mole of formula

unit $LaMg_2Ni$ can be expressed as follows:

$$G^{LaMg_2Ni} = {}^{\circ}G_{La}^{dhcp} + 2{}^{\circ}G_{Mg}^{hcp} + {}^{\circ}G_{Ni}^{fcc} + G_f \quad (3)$$

where ${}^{\circ}G_{La}^{dhcp}$, ${}^{\circ}G_{Mg}^{hcp}$ and ${}^{\circ}G_{Ni}^{fcc}$ are the Gibbs energies of the pure components dhcp-La, hcp-Mg and fcc-Ni, respectively, G_f is the Gibbs energy of formation of the stoichiometric phase referred to dhcp-La, hcp-Mg and fcc-Ni.

The binary stoichiometric compound La_2Mg_{17} has a Th_2Ni_{17}-type structure. In the La–Mg–Ni ternary system, this compound dissolves about 3 at.% Ni at constant La content since Ni atoms occupy the position of Mg atoms [24,32]. Therefore, it is treated as $(La)_2(Mg)_{14}(Mg,Ni)_3$.

The binary stoichiometric compound La_2Ni_7 can dissolve about 3 at.% Mg to form the solid solution $(La_{1-x}Mg_x)_2Ni_7$ at 773 K when Ni content keeps at a constant [32]. Dong et al. [3] and Zhang [28] also found that the La_2Ni_7 can dissolve about 5 at.% Mg at 1173 K. Thus, $(La_{1-x}Mg_x)_2Ni_7$ is treated as $(La, Mg)_2(Ni)_7$.

The solid solution $(La_{1-x}Mg_x)Ni_3$ at first was believed to be a ternary stoichiometric compound $LaMg_2Ni_9$ [27] with $PuNi_3$-type structure. Later, some researchers found that a series of alloys $(La_{1-x}Mg_x)Ni_3$ ($0 \le x \le 0.67$) had the same $PuNi_3$-type structure as $LaNi_3$. In this work, we refer to De Negri et al.'s opinion [32] that a continuous solid solution for the type $(La_{1-x}Mg_x)Ni_3$ exists in the range of $0 \le x \le 0.67$ forming by La/Mg substitution on the 6*c* site of the $R\bar{3}m$ space group. The $LaMg_2Ni_9$ stoichiometry, corresponding to $x = 0.67$, represents the Mg-richest composition of this phase, due to the saturation of the 6*c* site with Mg. The $(La_{1-x}Mg_x)Ni_3$ ($0 \le x \le 0.67$) is treated as $(La)_1(La, Mg)_2(Ni)_9$.

The solid solution $(La_{1-x}Mg_x)Ni_2$ was already reported by many researchers [9,25,26,31,32]. According to De Negri et al.'s opinion [31,32], the $(La_{1-x}Mg_x)Ni_2$ ternary phase can be described as a solid solution crystallizing in the $MgCu_4Sn$-type structure with a homogeneity range of $0 < x < 0.60$, where the 16*e* site in the space group $F\bar{4}3m$ is occupied by Ni, the 4*a* site by La and the 4*c* site by a disordered mixture of La and Mg in the range of $0 < x < 0.5$. For $LaMgNi_4$ ($x = 0.5$), the 4*c* site is likely to be saturated by Mg. In the range of $0.5 < x < 0.67$, a further Mg/La partial replacement occurred in the 4*a* site. When $x = 0$, the $LaNi_2$ binary phase is reported to be metastable in the La–Ni system. Actually, it may be stabilized by an Mg/La substitution in the ternary system. So, in this work, the $(La_{1-x}Mg_x)Ni_2$ ternary phase is treated as $(La, Mg)_1(Ni)_2$.

The Gibbs energies of the ordered intermetallic phases $La_2(Mg_{1-x}Ni_x)_{17}$, $(La_{1-x}Mg_x)Ni_2$, $(La_{1-x}Mg_x)Ni_3$ and $(La_{1-x}Mg_x)_2Ni_7$ could be described as the compound energy formalism with a three-sublattice model of $(p,q)_{f1}(r)_{f2}(s)_{f3}$, which Gibbs energy is

$$G = G^{ref} + G^{id} + G^{ex} \quad (4)$$

where G^{ref} is expressed in terms of compound energies and their associated sublattice species concentrations, y_p, y_q:

$$G^{ref} = y_p G_{(p:r:s)} + y_q G_{(q:r:s)} \quad (5)$$

G^{id} is the ideal mixing term, which is assumed to be random mixing of species on each sublattice:

$$G^{id} = f_1 \cdot RT[y_p \ln(y_p) + y_q \ln(y_q)] \quad (6)$$

The excess term G^{ex} is also expressed as a function of species concentrations with the sublattice *L* parameters being the numerical coefficients in the contributing terms:

$$G^{ex} = y_p y_q L_{(p,q:r:s)} \quad (7)$$

where

$$L_{(p,q:r:s)} = \sum_{\nu} L^{\nu}_{(p,q:r:s)} (y_p - y_q)^{\nu} \quad (8)$$

4. Thermodynamic assessment

Based on the binary sub-systems, the ternary database was constructed and assessed. The La–Mg–Ni ternary system was optimized using the available literature data. All the assessment and calculations were done using the Pandat Software [35]. All the obtained parameters and thermodynamic models were listed in Table 2.

4.1. Binary systems

The binary La–Mg, Mg–Ni and La–Ni systems have been optimized by Guo and Du [16], Jacobs and Spencer [18] and Du et al. [21], respectively. In order to assure the self-consistency, the diagrams were recalculated in this work, which showed a good agreement with the experimental phase equilibrium and the assessed thermodynamic data as presented in those studies. Their thermodynamic models and parameters are also summarized in Table 2.

4.2. Liquid

Experimentally determined enthalpies of mixing of liquid [29] were used to evaluate the ternary interaction parameters for the liquid phase. A temperature-dependent parameter could not obviously ameliorate the thermodynamic description, therefore it was omitted. Calculated and experimental values of the enthalpies of mixing are plotted in Fig. 1 for the sections of $La_{0.52}Ni_{0.48}$–Mg and $Mg_{0.79}Ni_{0.21}$–La at 1036 K. Good agreement can be observed.

4.3. The Mg–Ni side

The phase relationships in the Mg-rich corner at 673 K and 773 K have been investigated by Effenberg et al. [23] and De Negri et al. [31], respectively. Based on their experimental data, the Mg-rich corner was assessed. A discrepancy was found in the 673 K isothermal section between Effenberg et al.'s revised phase diagram [23] and the calculated result. Effenberg et al. [23] thought that La_5Mg_{41} can exist stably but Giovannini et al. [14] found that La_5Mg_{41} and La_2Mg_{17} could not coexist and only La_2Mg_{17} was stable. In the isothermal section at 773 K, a discrepancy resulted from the existence of liquid was between the calculated result and the experimental phase diagram reported by De Negri's et al. [31] (Fig. 2a), who did not find the appearance of the liquid, but the calculated result shows the liquid appears near the Mg–Ni binary boundary region. Due to the difficulty in detecting the liquid, so far no experiment was performed to confirm the existence of the liquid.

In the Ni-rich corner, we first assumed the melting temperatures of the $(La_{1-x}Mg_x)Ni_2$ ($x = 0.5$) and $(La_{1-x}Mg_x)Ni_3$ ($x = 0.67$) according to the experimental data. Kadir et al. [26] used the sintering method to prepare the $LaMgNi_4$ ternary compound, a mixture of the components in the atomic ratio of La:Mg:Ni = 1:1:4 was pressed to a plate and heat treated in a tube furnace at 973 K for 2 h. Zhang [34] had annealed $LaMgNi_4$ alloy at 1023 K for 24 h. Thermal effectiveness at 973 K and 1023 K revealed that the melting temperature of this ternary compound should be higher than 1023 K. So, in this work, the melting temperature of $LaMgNi_4$ was assumed to be 1133 K. Similarly, the melting temperature of $LaMg_2Ni_9$ was assumed to be 1473 K since the $LaMg_2Ni_9$ sample was prepared at 1373 K by Kadir et al. [27] using sintering method and $La_xMg_{3-x}Ni_9$ ($x = 1.0$–2.0) alloys were prepared at 1273 K by Liao et al. [2]. Based on the experimental data reported by De Negri et al. [31], Zhang [28], and Zhang [34], the thermodynamic model parameters in the Ni-rich corner were optimized.

Table 2
Thermodynamic parameters for the Mg–Ni side of La–Mg–Ni system reported in the literatures and optimized in this study (in J/mol of the formula unit).

Liquid:(La,Mg,Ni)$_1$	${}^0L^{\mathrm{Liq}}_{\mathrm{La,Mg}} = -32472.5 + 8.3674T$	[16]
	${}^1L^{\mathrm{Liq}}_{\mathrm{La,Mg}} = 35610.1 - 24.0118T$	[16]
	${}^2L^{\mathrm{Liq}}_{\mathrm{La,Mg}} = -13162.4$	[16]
	${}^0L^{\mathrm{Liq}}_{\mathrm{La,Ni}} = -116,299 + 19.815T$	[21]
	${}^1L^{\mathrm{Liq}}_{\mathrm{La,Ni}} = -63,813 + 40.941T$	[21]
	${}^0L^{\mathrm{Liq}}_{\mathrm{Mg,Ni}} = -50910.00 + 25.79995T$	[18]
	${}^1L^{\mathrm{Liq}}_{\mathrm{Mg,Ni}} = -14989.95 + 13.24788T$	[18]
	${}^0L^{\mathrm{Liq}}_{\mathrm{La,Mg,Ni}} = -15,000$	This work
Hcp-Mg:(La,Mg)$_1$	${}^0G^{\mathrm{Hcp}}_{\mathrm{La}} = {}^0G^{\mathrm{Dhcp}}_{\mathrm{La}} + 5000$	[16]
	${}^0L^{\mathrm{Hcp}}_{\mathrm{La,Mg}} = -25,000$	[16]
La_2Ni_3:(La)$_2$(Ni)$_3$	${}^0G^{\mathrm{La_2Ni_3}}_{\mathrm{La:Ni}} = 2{}^0G^{\mathrm{Dhcp}}_{\mathrm{La}} + 3{}^0G^{\mathrm{Fcc}}_{\mathrm{Ni}} - 138,509 + 14.109T$	[21]
La_7Ni_{16}:(La)$_7$(Ni)$_{16}$	${}^0G^{\mathrm{La_7Ni_{16}}}_{\mathrm{La:Ni}} = 7{}^0G^{\mathrm{Dhcp}}_{\mathrm{La}} + 16{}^0G^{\mathrm{Fcc}}_{\mathrm{Ni}} - 639,390 + 91.778T$	[21]
$LaNi_5$:(La)$_1$(Ni)$_5$	${}^0G^{\mathrm{LaNi_5}}_{\mathrm{La:Ni}} = {}^0G^{\mathrm{Dhcp}}_{\mathrm{La}} + 5{}^0G^{\mathrm{Fcc}}_{\mathrm{Ni}} - 154,674 + 30.662T$	[21]
$LaMg_{12}$:(La,Mg)$_1$(La,Mg)$_{12}$	${}^0G^{\mathrm{LaMg_{12}}}_{\mathrm{La:Mg}} = {}^0G^{\mathrm{Dhcp}}_{\mathrm{La}} + 12{}^0G^{\mathrm{Hcp}}_{\mathrm{Mg}} - 83174.4 + 16.9515T$	[16]
	${}^0G^{\mathrm{LaMg_{12}}}_{\mathrm{Mg:La}} = 12{}^0G^{\mathrm{Dhcp}}_{\mathrm{La}} + {}^0G^{\mathrm{Hcp}}_{\mathrm{Mg}} + 83174.4 - 16.9515T$	[16]
	${}^0G^{\mathrm{LaMg_{12}}}_{\mathrm{Mg:Mg}} = 13{}^0G^{\mathrm{Hcp}}_{\mathrm{Mg}} + 20,000$	[16]
	${}^0G^{\mathrm{LaMg_{12}}}_{\mathrm{La:La}} = 13{}^0G^{\mathrm{Dhcp}}_{\mathrm{La}} + 20,000$	[16]
	${}^0L^{\mathrm{LaMg_{12}}}_{\mathrm{La,Mg:La}} = {}^0L^{\mathrm{LaMg_{12}}}_{\mathrm{La,Mg:Mg}} = 9059.4 - 10.42T$	[16]
	${}^0L^{\mathrm{LaMg_{12}}}_{\mathrm{La:La,Mg}} = {}^0L^{\mathrm{LaMg_{12}}}_{\mathrm{Mg:La,Mg}} = -9061.1 + 11.9552T$	[16]
LaMg:(La)$_1$(Mg)$_1$	${}^0G^{\mathrm{LaMg}}_{\mathrm{La:Mg}} = {}^0G^{\mathrm{Dhcp}}_{\mathrm{La}} + {}^0G^{\mathrm{Hcp}}_{\mathrm{Mg}} - 33402.3 + 9.1880T$	[16]
$LaMg_2$:(La)$_1$(Mg)$_2$	${}^0G^{\mathrm{LaMg_2}}_{\mathrm{La:Mg}} = {}^0G^{\mathrm{Dhcp}}_{\mathrm{La}} + 2{}^0G^{\mathrm{Hcp}}_{\mathrm{Mg}} - 26814.7 - 10.1377T$	[16]
$LaMg_3$:(La,Mg)$_1$(Mg)$_3$	${}^0G^{\mathrm{LaMg_3}}_{\mathrm{La:Mg}} = {}^0G^{\mathrm{Dhcp}}_{\mathrm{La}} + 3{}^0G^{\mathrm{Hcp}}_{\mathrm{Mg}} - 78791.5 + 29.2136T$	[16]
	${}^0G^{\mathrm{LaMg_3}}_{\mathrm{Mg:Mg}} = 4{}^0G^{\mathrm{Hcp}}_{\mathrm{Mg}} + 5000$	[16]
	${}^0L^{\mathrm{LaMg_3}}_{\mathrm{La,Mg:Mg}} = 6797.4 - 3.7761T$	[16]
Mg_2Ni:(Mg)$_{0.6667}$(Ni)$_{0.3333}$	${}^0G^{\mathrm{Mg_2Ni}}_{\mathrm{Mg:Ni}} = -20320.40 + 138.49311T - 24.9354T\ln T - 1.538\times10^{-3}T^2 + 133,805T^{-1}$	[18]
$MgNi_2$:	${}^0G^{\mathrm{MgNi_2}}_{\mathrm{Mg:Ni}} = -24688.46 + 147.27013T - 25.7998T\ln T - 2.46496\times10^{-3}T^2 + 11575.5T^{-1}$	[18]
(Mg,Ni)$_{0.3333}$(Mg,Ni)$_{0.6667}$	${}^0G^{\mathrm{MgNi_2}}_{\mathrm{Mg:Mg}} = {}^0G^{\mathrm{Hcp}}_{\mathrm{Mg}} + 764.7058861 + 20.5882353T$	[18]
	${}^0G^{\mathrm{MgNi_2}}_{\mathrm{Ni:Mg}} = 0.6667{}^0G^{\mathrm{Hcp}}_{\mathrm{Mg}} + 0.3333{}^0G^{\mathrm{Fcc}}_{\mathrm{Ni}} + 1000$	[18]
	${}^0G^{\mathrm{MgNi_2}}_{\mathrm{Ni:Ni}} = {}^0G^{\mathrm{Fcc}}_{\mathrm{Ni}} + 5254.902 + 6.862745T$	[18]
$LaMg_2Ni$:(La)$_1$(Mg)$_2$(Ni)$_1$	${}^0G^{\mathrm{LaMg_2Ni}}_{\mathrm{La:Mg:Ni}} = {}^0G^{\mathrm{Dhcp}}_{\mathrm{La}} + 2{}^0G^{\mathrm{Hcp}}_{\mathrm{Mg}} + {}^0G^{\mathrm{Fcc}}_{\mathrm{Ni}} - 123074.7163 + 51.8431T$	This work
La_2Mg_{17}:(La)$_2$(Mg)$_{14}$(Mg,Ni)$_3$	${}^0G^{\mathrm{La_2Mg_{17}}}_{\mathrm{La:Mg:Mg}} = 2{}^0G^{\mathrm{Dhcp}}_{\mathrm{La}} + 17{}^0G^{\mathrm{Hcp}}_{\mathrm{Mg}} - 164604.6 + 39.3279T$	[16]
	${}^0G^{\mathrm{La_2Mg_{17}}}_{\mathrm{La:Mg:Ni}} = 2{}^0G^{\mathrm{Dhcp}}_{\mathrm{La}} + 14{}^0G^{\mathrm{Hcp}}_{\mathrm{Mg}} + 3{}^0G^{\mathrm{Fcc}}_{\mathrm{Ni}}$	This work
	${}^0L^{\mathrm{La_2Mg_{17}}}_{\mathrm{La:Mg:Mg,Ni}} = -464,600 + 200T$	This work
	${}^1L^{\mathrm{La_2Mg_{17}}}_{\mathrm{La:Mg:Mg,Ni}} = 217,300 - 100T$	This work
(La,Mg)Ni_2:(La,Mg)$_1$(Ni)$_2$	${}^0G^{\mathrm{(La,Mg)Ni_2}}_{\mathrm{La:Ni}} = {}^0G^{\mathrm{Dhcp}}_{\mathrm{La}} + 2{}^0G^{\mathrm{Fcc}}_{\mathrm{Ni}} - 82890.4953 + 10.5561T$	This work
	${}^0G^{\mathrm{(La,Mg)Ni_2}}_{\mathrm{Mg:Ni}} = -62865.38 + 441.81039T - 77.3994T\ln T - 7.39488\times10^{-3}T^2 + 334,726T^{-1}$	This work
	${}^0L^{\mathrm{(La,Mg)Ni_2}}_{\mathrm{La:Mg,Ni}} = -77,055 + 35T$	This work
(La,Mg)Ni_3:	${}^0G^{\mathrm{(La,Mg)Ni_3}}_{\mathrm{La:La:Ni}} = 3{}^0G^{\mathrm{Dhcp}}_{\mathrm{La}} + 9{}^0G^{\mathrm{Fcc}}_{\mathrm{Ni}} - 324,462 + 47.571T$	[21]
(La)$_1$(La,Mg)$_2$(Ni)$_9$	${}^0G^{\mathrm{(La,Mg)Ni_3}}_{\mathrm{La:Mg:Ni}} = {}^0G^{\mathrm{Dhcp}}_{\mathrm{La}} + 2{}^0G^{\mathrm{Hcp}}_{\mathrm{Mg}} + 9{}^0G^{\mathrm{Fcc}}_{\mathrm{Ni}} - 260356.9427 + 45.7399T$	This work
	${}^0L^{\mathrm{(La,Mg)Ni_2}}_{\mathrm{La:La,Mg:Ni}} = -127,300 + 100T$	This work
	${}^0L^{\mathrm{(La,Mg)Ni_2}}_{\mathrm{La:La,Mg:Ni}} = -30,000$	This work
α(La,Mg)$_2Ni_7$:(La,Mg)$_2$(Ni)$_7$	${}^0G^{\alpha\mathrm{(La,Mg)_2Ni_7}}_{\mathrm{La:Ni}} = 2{}^0G^{\mathrm{Dhcp}}_{\mathrm{La}} + 7{}^0G^{\mathrm{Fcc}}_{\mathrm{Ni}} - 239,869 + 37.356T$	[21]
	${}^0G^{\alpha\mathrm{(La,Mg)_2Ni_7}}_{\mathrm{Mg:Ni}} = 2{}^0G^{\mathrm{Hcp}}_{\mathrm{Mg}} + 7{}^0G^{\mathrm{Fcc}}_{\mathrm{Ni}}$	This work
	${}^0L^{\alpha\mathrm{(La,Mg)_2Ni_7}}_{\mathrm{La,Mg:Ni}} = -296,625 + 125\,T$	This work
β(La,Mg)$_2Ni_7$:(La,Mg)$_2$(Ni)$_7$	${}^0G^{\beta\mathrm{(La,Mg)_2Ni_7}}_{\mathrm{La:Ni}} = 2{}^0G^{\mathrm{Dhcp}}_{\mathrm{La}} + 7{}^0G^{\mathrm{Fcc}}_{\mathrm{Ni}} - 237,259 + 35.267T$	[21]
	${}^0G^{\beta\mathrm{(La,Mg)_2Ni_7}}_{\mathrm{Mg:Ni}} = 2{}^0G^{\mathrm{Hcp}}_{\mathrm{Mg}} + 7{}^0G^{\mathrm{Fcc}}_{\mathrm{Ni}}$	This work
	${}^0L^{\beta\mathrm{(La,Mg)_2Ni_7}}_{\mathrm{La,Mg:Ni}} = -296,625 + 125T$	This work

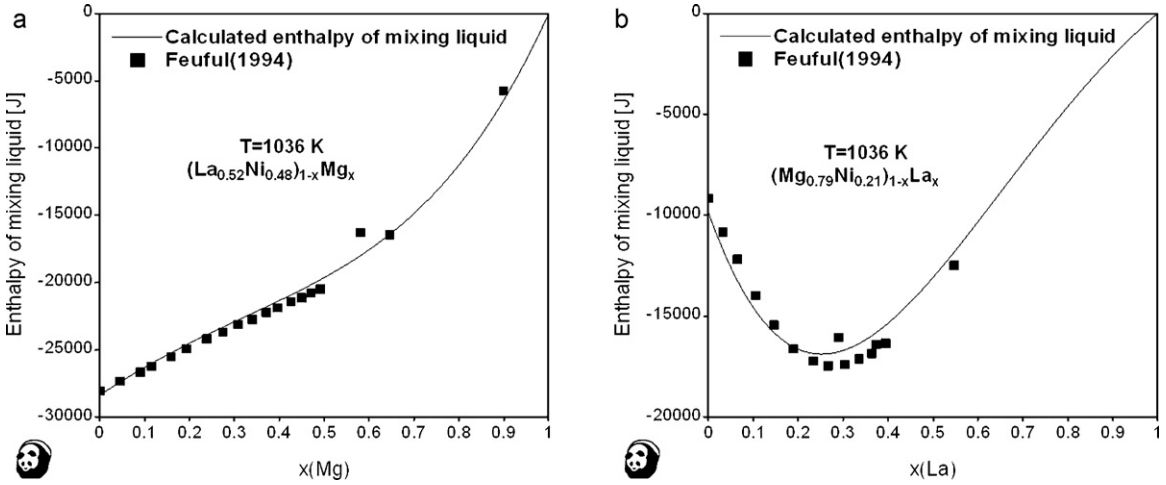

Fig. 1. Calculated enthalpies of mixing of liquid $(La_{0.52}Ni_{0.48})_{1-x}Mg_x$ (a) and $(Mg_{0.79}Ni_{0.21})_{1-x}La_x$ (b) and experimental results at 1036 K.

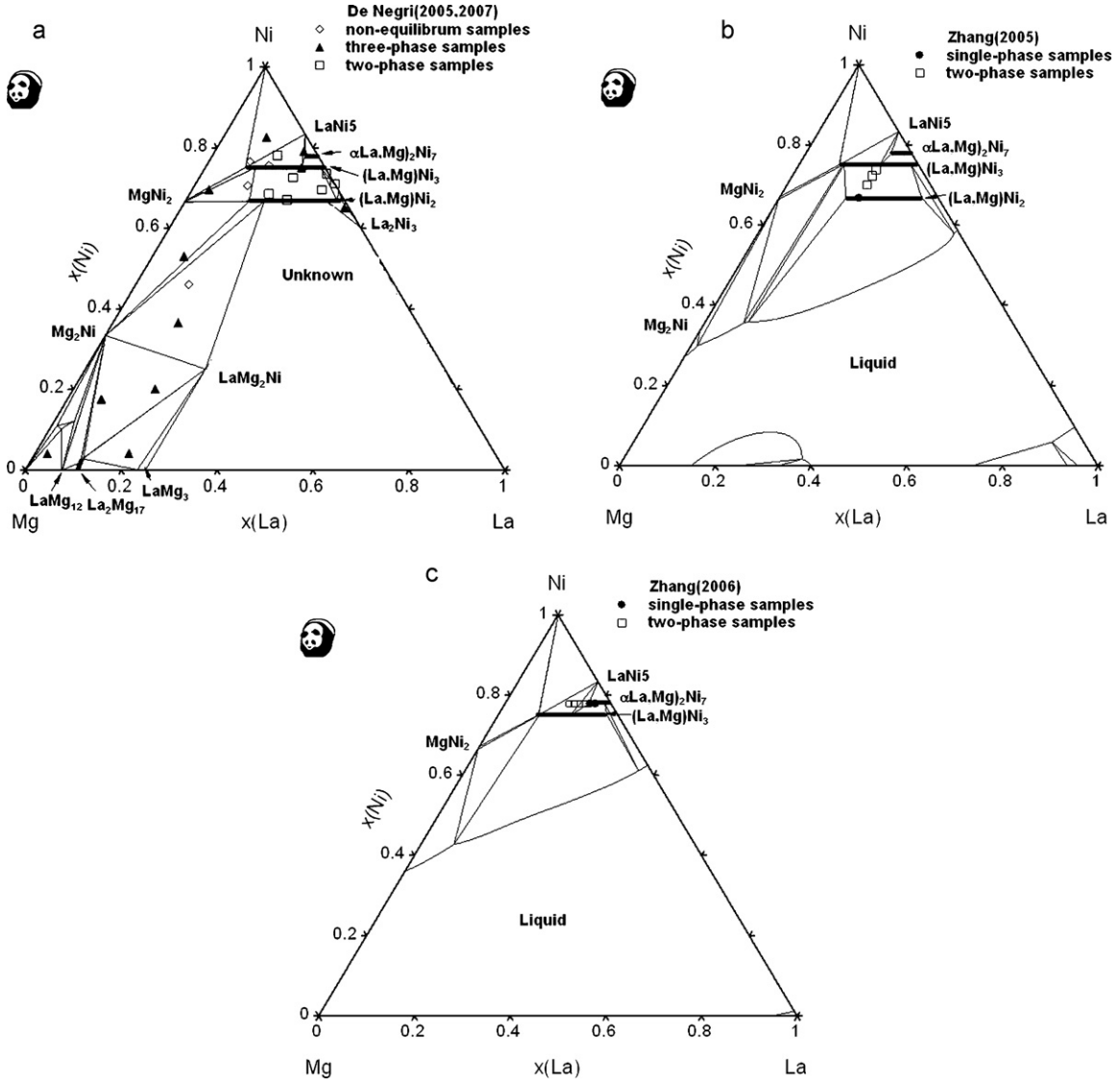

Fig. 2. Calculated isothermal sections of Mg–Ni side at 773 K (a), 1023 K (b) and 1173 K (c) and experimental points reported by De Negri et al. [31,32], Zhang [28] and Zhang [34].

Table 3
Predicted invariant reactions at the Mg–Ni side of the La–Mg–Ni system.

Reaction	T (K)	Composition in liquid		
		x (La)	x (Mg)	x (Ni)
Liq. → (La,Mg)Ni_3 + (Ni) + $LaNi_5$	1422	0.0590	0.0937	0.8473
Liq. + $LaNi_5$ → (La,Mg)Ni_3 + β(La,Mg)$_2Ni_7$	1370	0.1875	0.1615	0.6510
Liq. → (La,Mg)Ni_3 + (Ni) + $MgNi_2$	1359	0.0104	0.1934	0.7962
Liq. + (La,Mg)Ni_3 → (La,Mg)Ni_2 + $MgNi_2$	1008	0.0824	0.5676	0.3500
Liq. + (La,Mg)Ni_3 → (La,Mg)Ni_2 + La_7Ni_{16}	979	0.4212	0.0010	0.5778
Liq. + La_7Ni_{16} → (La,Mg)Ni_2 + La_2Ni_3	960	0.4282	0.0003	0.5715
Liq. + $MgNi_2$ → (La,Mg)Ni_2 + Mg_2Ni	949	0.0748	0.6089	0.3163
Liq. + (La,Mg)Ni_2 → Mg_2Ni + $LaMg_2Ni$	834	0.1171	0.6232	0.2597
Liq. + $LaMg_3$ → $LaMg_2Ni$ + LaMg	791	0.5005	0.2129	0.2866
Liq. + $LaMg_3$ → $LaMg_2Ni$ + La_2Mg_{17}	788	0.0901	0.7561	0.1538
Liq. → Mg_2Ni + $LaMg_2Ni$ + La_2Mg_{17}	778	0.0838	0.7577	0.1585
Liq. + La_2Mg_{17} → Mg_2Ni + $LaMg_{12}$	773	0.0420	0.8365	0.1215
Liq. → (Mg) + Mg_2Ni + $LaMg_{12}$	760	0.0228	0.8687	0.1085

4.4. Calculated results

Considering the properties of the liquid and the phase relationships in the Mg-rich corner and Ni-rich corner, the thermodynamic description of the Mg–Ni side in the La–Mg–Ni system was obtained. Fig. 2a shows the calculated isothermal section at 773 K and the experimental points reported by De Negri et al. [31,32], they thought the solubility ranges of the $(La_{1-x}Mg_x)Ni_2$, $(La_{1-x}Mg_x)Ni_3$ and $(La_{1-x}Mg_x)_2Ni_7$ at 773 K were $0 < x \leq 0.6$, $0 \leq x \leq 0.67$ and $0 \leq x \leq 0.13$, respectively. Fig. 2b shows the calculated isothermal section at 1023 K and the experimental points reported by Zhang [34], who successfully detected the single-phase region $LaMgNi_4$ and the two-phase region $(La_{1-x}Mg_x)Ni_2$ + $(La_{1-x}Mg_x)Ni_3$ at 1023 K. Fig. 2c shows the calculated isothermal section of Mg–Ni side at 1173 K and the experimental points reported by Zhang [28], who prepared a series of $La_{2-x}Mg_xNi_7$ ($0.3 \leq x \leq 0.8$) hydrogen storage alloys and found that the maximal solubility range of $(La_{1-x}Mg_x)_2Ni_7$ was between $x = 0.4$ and $x = 0.5$. The predicted invariant equilibria on the liquidus surface at the Mg–Ni side of the La–Mg–Ni system are listed in Table 3.

In addition, there should exist a two-phase region Ni + (La,Mg)Ni_3 between the two three-phase regions (La,Mg)Ni_3 + (Ni) + $MgNi_2$ and (La,Mg)Ni_3 + $LaNi_5$ + (Ni). In fact, the two-phase region Ni + (La,Mg)Ni_3 indeed exists in the calculated phase diagram but appears to be a very narrow line.

5. Experimental verification

5.1. Experimental detail

In order to prove the calculated phase diagram by CALPAHD approach, the verification test was carried out. The first step was to select the key specimens and molten alloys. Ni 99.99 mass% purity, Mg 99.99 mass% purity, and La 99.83 mass% purity were used as the starting materials. The ternary alloys were prepared by induction melting under an argon atmosphere. In order to control the material loss due to the volatilization of Mg, the La–Ni binary intermediate alloys were firstly prepared, and then Mg was added. These prepared alloys were generally annealed in evacuated quartz ampoules at 773 K, 973 K and 1173 K for 30 days, respectively. All samples were quenched in cold water and their elemental compositions were determined using the element chemical analysis by inductively coupled plasma (ICP) in order to detect the difference between the nominal composition and the actual composition.

Both as-cast and annealed samples were investigated by XRD analysis on a DLMAX-2200 diffractometer (CuKα radiation). The Materials Data Inc. software Jade 5.0 and a Powder Diffraction File (PDF release 2002) were used to analyze the XRD data. Some key alloys were further investigated by scanning electron microscopy (SEM, JSM-6700F).

5.2. Results and discussion

Table 4 lists the compositions and XRD characterizations of samples No. 1–16. All experimental results in Table 4 also marked in Figs. 3, 5 and 6 in order to compare with the calculated results. Fig. 3 shows the calculated isothermal section at 773 K with marked samples No. 1–4 annealed at 773 K. The results of the XRD and SEM characterizations for samples No. 1–4 show a good agreement with the phase relationships of the calculated isothermal section at 773 K. The microphotographs of two selected alloys are shown in Fig. 4, from which it can be seen that an typical eutectic struc-

Table 4
Results of the XRD characterization of selected La–Mg–Ni alloys annealed at 773 K, 973 K and 1173 K.

Sample/composition	Annealing temperature	Phase analysis
No. 1/$La_{14.00}Mg_{44.00}Ni_{42.00}$	773 K	$LaMg_2Ni$, (La,Mg)Ni_2, Mg_2Ni
No. 2/$La_{3.00}Mg_{17.00}Ni_{80.00}$	773 K	(La,Mg)Ni_3, (Ni), $MgNi_2$
No. 3/$La_{10.00}Mg_{5.40}Ni_{84.60}$	773 K	(La,Mg)Ni_3, (Ni), $LaNi_5$
No. 4/$La_{4.00}Mg_{41.00}Ni_{55.00}$	773 K	(La,Mg)Ni_2, Mg_2Ni, $MgNi_2$
No. 5/$La_{3.00}Mg_{17.00}Ni_{80.00}$	973 K	(La,Mg)Ni_3, (Ni), $MgNi_2$
No. 6/$La_{10.00}Mg_{5.40}Ni_{84.60}$	973 K	(La,Mg)Ni_3, (Ni), $LaNi_5$
No. 7/$La_{9.00}Mg_{22.00}Ni_{69.00}$	973 K	(La,Mg)Ni_2, (La,Mg)Ni_3, $MgNi_2$, $LaNi_5$
No. 8/$La_{13.08}Mg_{9.93}Ni_{76.99}$	973 K	(La,Mg)Ni_3, $LaNi_5$
No. 9/$La_{12.63}Mg_{5.80}Ni_{81.57}$	973 K	(La,Mg)Ni_3, $LaNi_5$, (Ni)
No. 10/$La_{8.00}Mg_{12.67}Ni_{79.33}$	973 K	(La,Mg)Ni_3, $LaNi_5$, (Ni)
No. 11/$La_{9.49}Mg_{12.24}Ni_{78.28}$	973 K	(La,Mg)Ni_3, $LaNi_5$, (Ni)
No. 12/$La_{3.00}Mg_{17.00}Ni_{80.00}$	1173 K	(La,Mg)Ni_3, (Ni), $MgNi_2$
No. 13/$La_{10.00}Mg_{5.40}Ni_{84.60}$	1173 K	(La,Mg)Ni_3, (Ni), $LaNi_5$
No. 14/$La_{10.91}Mg_{0.04}Ni_{89.05}$	1173 K	(La,Mg)Ni_3, (Ni), $LaNi_5$
No. 15/$La_{9.52}Mg_{7.58}Ni_{82.90}$	1173 K	(La,Mg)Ni_3, (Ni), $LaNi_5$
No. 16/$La_{10.72}Mg_{5.54}Ni_{83.74}$	1173 K	(La,Mg)Ni_3, (Ni), $LaNi_5$

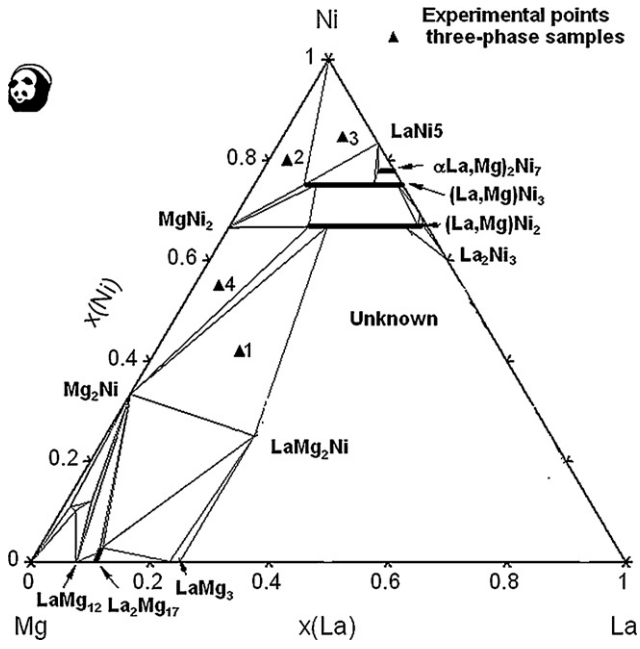

Fig. 3. Calculated isothermal section at 773 K with the experimental results marked samples No. 1–4.

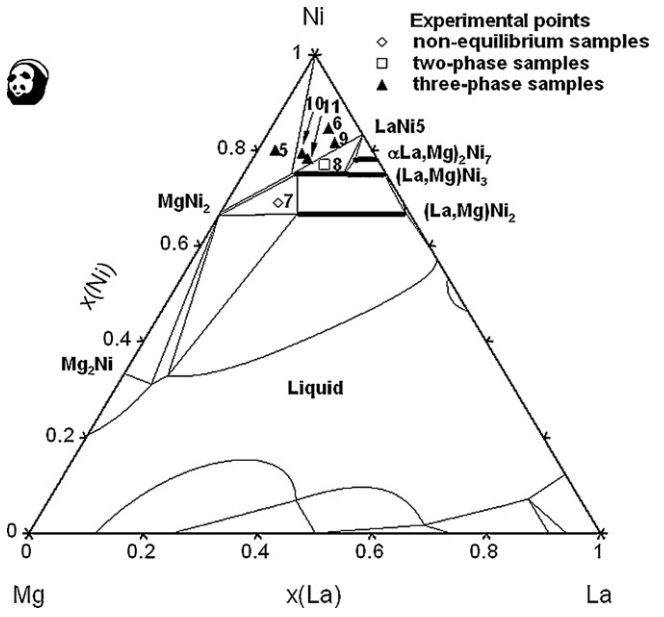

Fig. 5. Calculated isothermal section at 973 K with the experimental results marked samples No. 5–11.

ture, $(La,Mg)Ni_3 + (Ni)$, which is corresponding to the reaction of $Liq. \rightarrow (La,Mg)Ni_3 + (Ni) + LaNi_5$.

Fig. 5 shows the calculated isothermal section at 973 K with marked samples No. 5–11. The results of the XRD characterization for samples No. 5–11 also show a good agreement with the calculated isothermal section except sample No. 7, in which the $LaNi_5$ phase exists after annealing at 973 K. It is not consistent with the calculated phase diagram. It should be mentioned that De Negri et al. [31] also did not get the equilibrium phases by annealing at 773 K in the same phase region ($(La,Mg)Ni_3 + (La,Mg)Ni_2 + MgNi_2$). This may be caused by the coexistence of $(La,Mg)Ni_3$ and $LaNi_5$ phase, which is hard to be eliminated by annealing treatment. Sample No.10 shows that the two-phase region $(Ni) + (La,Mg)Ni_3$ between $(La,Mg)Ni_3 + (Ni) + MgNi_2$ and $(La,Mg)Ni_3 + LaNi_5 + (Ni)$ is indeed narrow as shown in the calculated diagram. Fig. 6 shows the calculated isothermal section at 1173 K with marked samples No. 12–16. The results of the XRD characterization for samples No. 12–16 show a good agreement with the calculated isothermal sections.

Comparison all the experimental results with the calculated results suggests that the assessed thermodynamic description of phase relationship has a good self-consistency.

6. Application

The thermodynamic modeling of the phase equilibria at the Mg–Ni side of the La–Mg–Ni ternary system in present paper can provide some valuable guidance for design of new materials and development of La–Mg–Ni hydrogen storage alloys. The obtained phase diagram mentioned above would be used to discuss the synthesized technological parameter of the La–Mg–Ni hydrogen storage alloys, which were verified by the experimental results published in literatures. Fig. 3 shows that several hydrogen storage phases with a high hydrogen storage capacity, e.g. Mg (7.6 wt.% H_2), $LaMg_{12}$ (6.0 wt.% H_2), La_2Mg_{17} (6.6 wt.% H_2) and Mg_2Ni (3.6 wt.% H_2), exist the Mg-rich corner of the La–Mg–Ni ternary system. The final phases in $La_{1.30}Mg_{92.22}Ni_{6.48}$ and $La_{2.10}Mg_{87.37}Ni_{10.53}$ are $(Mg) + Mg_2Ni + LaMg_{12}$, and that in $La_{4.21}Mg_{74.78}Ni_{21.01}$ are $La_2Mg_{17} + Mg_2Ni$ [36]. The phase relationships of these samples prepared from the mixture Mg and $LaNi_5$

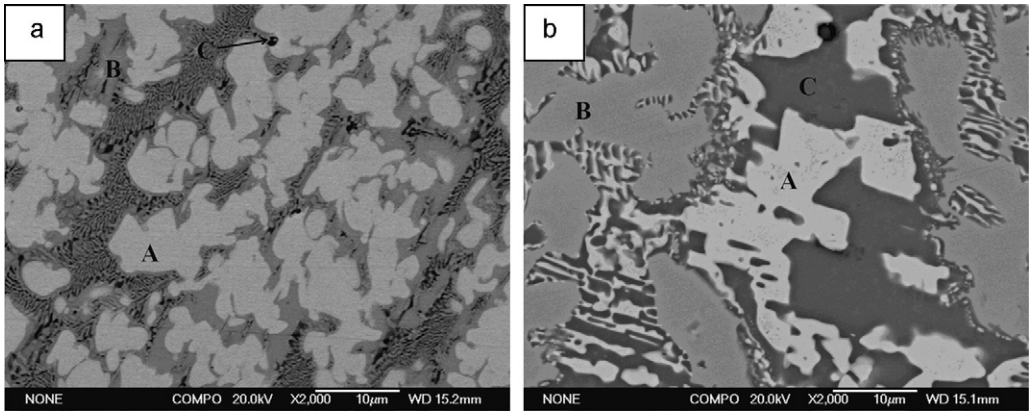

Fig. 4. SEM image (BSE mode) of the microstructure of sample No. 3 (a) [A: $LaNi_5$; B: $(La_{1-x}Mg_x)Ni_3$, $x = 0.67$; C: (Ni)] and sample No. 4 (b) [A: $(La_{1-x}Mg_x)Ni_2$; B: $MgNi_2$; C: Mg_2Ni] annealed at 773 K.

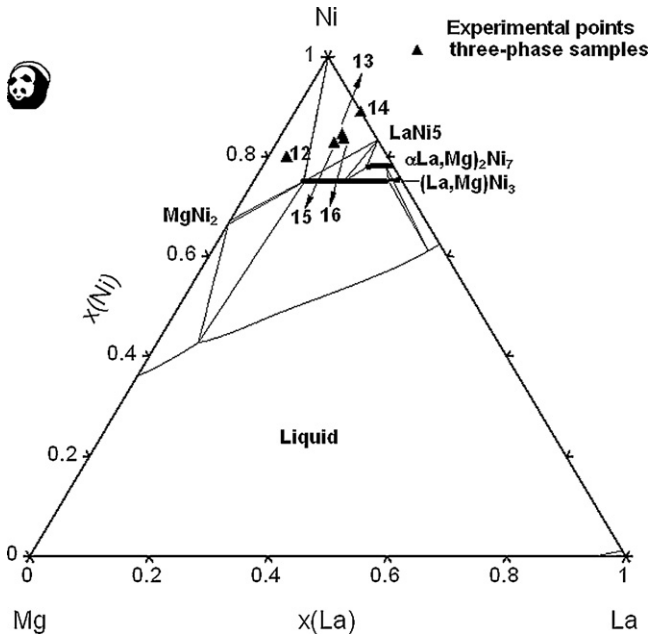

Fig. 6. Calculated isothermal section at 1173 K with the experimental results marked samples No. 12–16.

agree well with our calculated results. Fig. 7 clearly shows the vertical section of these samples. All the samples show a better activation behavior under a pressure of 5 MPa at 623 K than pure Mg, which is associated with the presence of secondary phases, such as the Mg_2Ni, $LaMg_{12}$ and La_2Mg_{17}. The maximum hydrogen concentration can reach to 5.6 wt.% H_2 and decrease with the decrease of the phase abundance of pure Mg. In the Ni-rich corner, the La–Mg–Ni hydrogen storage alloys usually show good electrochemical properties due to the existence of the $LaNi_5$, $(La_{1-x}Mg_x)_2Ni_7$ and $(La_{1-x}Mg_x)Ni_3$. Zhang et al. [37] studied the electrochemical behaviors of $La_{0.75}Mg_{0.25}Ni_{3.5}M_x$ (M = Ni; x = 0–0.6) hydrogen storage alloys composed of $(La_{1-x}Mg_x)Ni_3$ and $LaNi_5$, which are well agreed with our calculated vertical section showed in Fig. 8. All the hydrogen storage alloys exhibit good integrative electrochemical performances including a high dis-

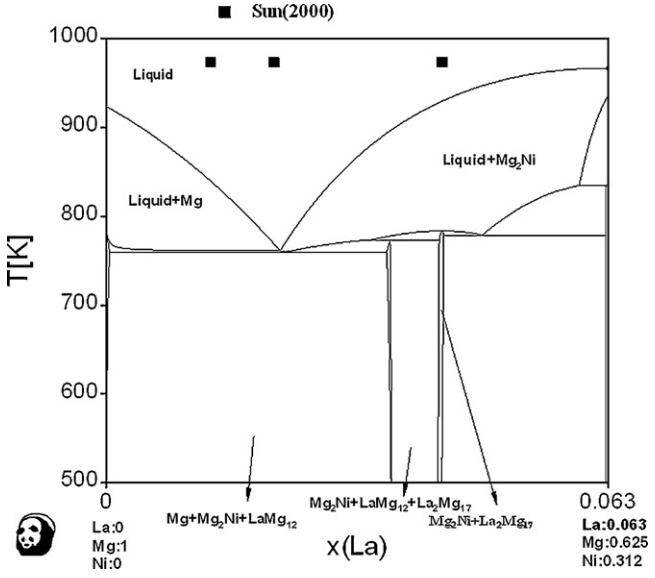

Fig. 7. Calculated partial vertical section Mg–$LaNi_5$ with the experimental points reported by Sun et al. [36].

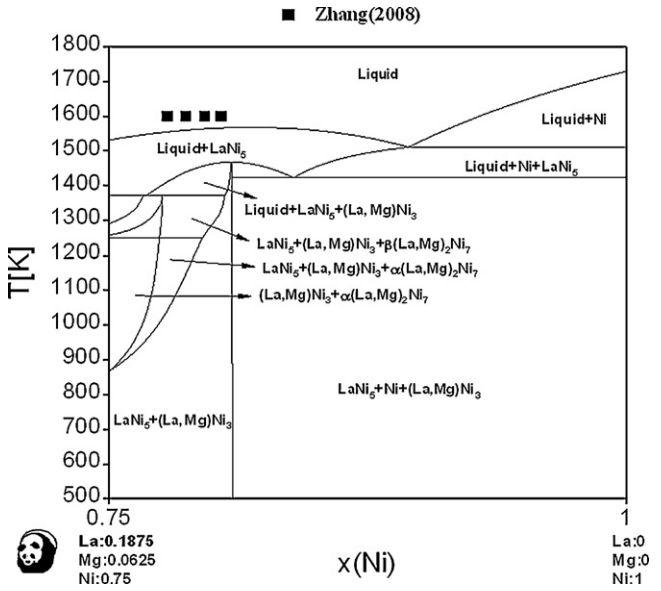

Fig. 8. Calculated partial vertical section $La_{0.75}Mg_{0.25}$–Ni with the experimental points reported by Zhang et al. [37].

charge capacity and a good capacity retaining rate, which have a closed relationship with phase composition of the termination product.

7. Conclusion

Based on available literature data, the Mg–Ni side in the La–Mg–Ni system was thermodynamically assessed and an optimal set of thermodynamic parameters was obtained. The phases of liquid, $La_2(Mg_{1-x}Ni_x)_{17}$, $LaMg_2Ni$, $(La_{1-x}Mg_x)Ni_2$, $(La_{1-x}Mg_x)Ni_3$ and $(La_{1-x}Mg_x)_2Ni_7$ were modeled and the thermodynamic parameters were optimized. Guided by the calculated results, sixteen specimens were melted in an induction furnace and annealed at 773 K, 973 K and 1173 K for 30 days to validate the calculated isothermal sections. The calculated Mg–Ni side of the La–Mg–Ni ternary system phase diagrams showed a good consistency with experimental results. The phase relationships of several key hydrogen storage phases containing Mg_2Ni, $LaNi_5$, $La_2(Mg_{1-x}Ni_x)_{17}$, $(La_{1-x}Mg_x)Ni_3$, $(La_{1-x}Mg_x)Ni_2$, $(La_{1-x}Mg_x)_2Ni_7$ and $LaMg_2Ni$ were detected in the present work. The calculated phase diagram was successfully used to discuss the synthesized technological parameter of the La–Mg–Ni hydrogen storage alloys.

Acknowledgments

The authors gratefully acknowledge the financial supports from the National Natural Science Foundation of China (50804029), Science and Technology Commission of Shanghai Municipality (09195802700) and the Program for Changjiang Scholars and Innovative Research Team in University (IRT0739).

References

[1] H. Ding, S. Han, Y. Liu, J. Hao, Y. Li, J. Zhang, Int. J. Hydrogen Energy 34 (2009) 9402–9408.
[2] B. Liao, Y.O. Lei, G.L. Lu, L.X. Chen, H.G. Pan, Q.D. Wang, J. Alloys Compd. 356–357 (2003) 746–749.
[3] X.P. Dong, F.X. Lü, Y.H. Zhang, L.Y. Yang, X.L. Wang, Mater. Chem. Phys. 108 (2008) 251–256.
[4] Y. Zhao, M.X. Gao, Y.F. Liu, L. Huang, H.G. Pan, J. Alloys Compd. 496 (2010) 454–461.
[5] X.L. Wang, X.P. Dong, Y.H. Zhang, S.H. Guo, F.X. Lü, J. Rare Earths 26 (2008) 284–290.

[6] J. Liu, X. Zhang, Q. Li, K.C. Chou, K.D. Xu, Int. J. Hydrogen Energy 34 (2009) 1951–1957.
[7] L. Schlapbach, A. Züttel, Nature 414 (2001) 353–358.
[8] M. Di Chio, A. Ziggiotti, M. Baricco, Intermetallics 16 (2008) 102–106.
[9] H. Oesterreicher, H. Bittner, J. Less-Common Met. 73 (1980) 339–344.
[10] R.V. Denys, I. Yu Zavaliy, V. Paul-boncoue, V.V. berezovets, I.V. Koval'chuk, A.B. Riabov, Intermetallics 18 (2010) 1579–1585.
[11] J.M. Joubert, Int. J. Hydrogen Energy 35 (2010) 2104–2111.
[12] K. Zeng, T. Klassen, W. Oelerich, R. Bormann, Int. J. Hydrogen Energy 24 (1999) 989–1004.
[13] A.A. Nayeb-Hashemi, J.B. Clark, Bull. Alloy Phase Diagram 9 (1988) 172–173.
[14] M. Giovannini, A. Saccone, R. Marazza, R. Ferro, Metall. Mater. Trans. A 26 (1995) 5–10.
[15] H. Okamoto, J. Phase Equilib. 14 (1993) 316–335.
[16] C.P. Guo, Z.M. Du, J. Alloys Compd. 385 (2004) 109–113.
[17] A.A. Nayeb-Hashemi, J.B. Clark, Bull. Alloy Phase Diagram 6 (1985) 238–244.
[18] M.H.G. Jacobs, P.J. Spencer, Calphad 22 (1998) 513–525.
[19] F. Islam, M. Medraj, Calphad 29 (2005) 289–302.
[20] H. Okamoto, J. Phase Equilib. 12 (1991) 615–616.
[21] Z. Du, D. Wang, W. Zhang, J. Alloys Compd. 264 (1998) 209–213.
[22] J. Dischinger, H.J. Schaller, J. Alloys Compd. 312 (2000) 201–210.
[23] G.F. Effenberg, F. Aldinger, P. Rogl, Ternary Alloys, MSI, Stuttgart (Federal Republic of Germany), 2001, p. 18.
[24] V.V. Karonic, D.N. Kazakov, R.A. Andrievskii, O.N. Bogachkova, Inorg. Mater. 20 (1984) 207–211.
[25] L. Guénée, V. Favre-Nicolin, K. Yvon, J. Alloys Compd. 348 (2003) 129–137.
[26] K. Kadir, D. Noréus, I. Yamashita, J. Alloys Compd. 345 (2002) 140–143.
[27] K. Kadir, T. Sakai, I. Uehara, J. Alloys Compd. 257 (1997) 115–121.
[28] F.L. Zhang, Doctoral Dissertation, Lanzhou University of Technology, Lanzhou, China, 2006, pp. 28–56.
[29] H. Feufel, M. Krishnaiah, F. Sommer, B. Predel, J. Phase Equilib. 15 (1994) 303–309.
[30] J. Schmid, F. Sommer, J. Alloys Compd. 266 (1998) 216–223.
[31] S. De Negri, M. Giovannini, A. Saccone, J. Alloys Compd. 397 (2005) 126–134.
[32] S. De Negri, M. Giovannini, A. Saccone, J. Alloys Compd. 439 (2007) 109–113.
[33] L.G. Zhang, H.Q. Dong, J.F. Nie, F.G. Meng, S. Jin, L.B. Liu, Z.P. Jin, J. Alloys Compd. 491 (2009) 123–130.
[34] Y. Zhang, Master's Dissertation, Lanzhou University of Technology, Lanzhou, China, 2005, pp. 33–48.
[35] S.L. Chen, S. Daniel, F. Zhang, Y.A. Chang, X.Y. Yan, F.Y. Xie, R. Schmid-Fetzer, W.A. Oates, Calphad 26 (2002) 175–188.
[36] D. Sun, F. Gingl, H. Enoki, D.K. Ross, E. Akiba, Acta Mater. 48 (2000) 2363–2372.
[37] Y.H. Zhang, X.P. Dong, D.L. Zhao, S.H. Guo, Y. Qi, X.L. Wang, Trans. Nonferrous Met. Soc. China 18 (2008) 857–864.